Cdc42 interacts with the exocyst complex to promote phagocytosis

Sina Mohammadi[2] and Ralph R. Isberg[1,2]

[1]Howard Hughes Medical Institute and [2]Department of Molecular Biology and Microbiology, Tufts University School of Medicine, Boston, MA 02111

The process of phagocytosis in multicellular organisms is required for homeostasis, clearance of foreign particles, and establishment of long-term immunity, yet the molecular determinants of uptake are not well characterized. Cdc42, a Rho guanosine triphosphatase, is thought to orchestrate critical actin remodeling events needed for internalization. In this paper, we show that Cdc42 controls exocytic events during phagosome formation. Cdc42 inactivation led to a selective defect in large particle phagocytosis as well as a general decrease in the rate of membrane flow to the cell surface. Supporting the connection between Cdc42 and exocytic function, we found that the overproduction of a regulator of exocytosis, Rab11, rescued the large particle uptake defect in the absence of Cdc42. Additionally, we demonstrated a temporal interaction between Cdc42 and the exocyst complex during large particle uptake. Furthermore, disruption of exocyst function through Exo70 depletion led to a defect in large particle internalization, thereby establishing a functional role for the exocyst complex during phagocytosis.

Introduction

Internalization of particles >0.5 µm is commonly referred to as phagocytosis, a process that is essential for homeostasis and immune defense. The requirement for phagocytosis in maintaining homeostatic balance is first manifested during embryonic development (Kerr et al., 1972) in which dead cells are cleared through phagocytosis to ensure proper organ sculpture (Vaux and Korsmeyer, 1999) and continues unabated after birth during which large numbers of cells (10^8–10^9) undergo apoptosis every day and need to be cleared (Ren and Savill, 1998). Phagocytosis is also crucially important in combating disease. In addition to destroying invading pathogens, phagocytes create a bridge between innate and acquired immunity by presenting antigens to T cells, thereby enabling the development of long-term immunity (Savina and Amigorena, 2007). The crucial roles phagocytosis plays in homeostasis and immunity make it one of the most fundamental processes in multicellular organisms.

Integrin- and Fc receptor (FcR)–mediated uptake are examples of receptor-mediated phagocytosis, through which particles are internalized into membrane-bound vacuoles called phagosomes. FcRs mediate uptake of antibody-opsonized particles (e.g., invading pathogens; Aderem and Underhill, 1999), and integrins mediate internalization and adhesion by binding to a diverse cadre of ligands (Hynes, 2002; Dupuy and Caron, 2008). For example, uptake of apoptotic cells involves integrin-mediated phagocytosis (Savill et al., 2002). Additionally, the bacterial pathogen *Yersinia pseudotuberculosis* enters both phagocytic and nonphagocytic cells by integrin-mediated uptake through the action of the surface protein invasin. Invasin binds tightly to β1 integrins at the same site as the cell adhesion ligand fibronectin (Tran Van Nhieu and Isberg, 1993) and is sufficient for mediating uptake (Rankin et al., 1992). Both integrin- and FcR-mediated uptake require the generation of contractile force by actin polymerization for membrane to surround the phagocytic particle (Dupuy and Caron, 2008; Swanson, 2008).

A complex array of signaling molecules is involved in orchestrating the actin polymerization during engulfment. Several Rho GTPases have been implicated in phagocytosis, though the set of Rho GTPases involved in this process depends on the phagocytic event studied. For instance, bacterial uptake promoted by invasin or uptake of *Salmonella enterica* serovar Typhimurium

Correspondence to Ralph R. Isberg: Ralph.Isberg@tufts.edu

Abbreviations used in this paper: CBD, Cdc42-binding domain; FcR, Fc receptor; FRET, fluorescence resonance energy transfer; KD, knockdown; MBP, maltose-binding protein; MEF, mouse embryonic fibroblast; NWASP, neural WASP; PBD, p21-binding domain; RE, recycling endosome; ROI, region of interest; shCdc42, Cdc42 shRNA; shScr, scrambled shRNA; TfR, transferrin receptor; WASP, Wiskott–Aldrich syndrome protein.

The Rockefeller University Press $30.00
J. Cell Biol. Vol. 200 No. 1 81–93
www.jcb.org/cgi/doi/10.1083/jcb.201204090

appears to occur in a Rac1- and RhoG-dependent and Cdc42-independent fashion (Patel and Galán, 2006; Mohammadi and Isberg, 2009). In contrast, uptake of antibody-coated erythrocytes requires both Cdc42 (Caron and Hall, 1998) and its downstream signaling molecules Wiskott–Aldrich syndrome protein (WASP) and neural WASP (NWASP; Park and Cox, 2009), with spatiotemporal activation of Cdc42 occurring during the uptake of erythrocytes (Beemiller et al., 2010). Integrin-mediated cell adhesion and spreading similarly requires several Rho GTPases, including Cdc42 (Clark et al., 1998; Price et al., 1998; Partridge and Marcantonio, 2006).

The processes of phagocytosis and cell adhesion and spreading involve many of the same molecular determinants and share similar signaling patterns during encounter with ligands (Cougoule et al., 2004). In fact, cell spreading could be viewed as the frustrated phagocytosis of an infinitely large particle. Furthermore, both processes require membrane delivery from internal sources to the cell surface (Cox et al., 1999; Gauthier et al., 2009). It was previously assumed that cell size decreases during phagocytosis. However, electrophysiological measurements and cell spreading assays have shown that cell surface area in fact increases (Holevinsky and Nelson, 1998; Cox et al., 1999). This increase is believed to be a result of membrane delivery from internal sources to the site of particle uptake, which has been termed focal exocytosis (Huynh et al., 2007). The recycling endosome (RE) is a major source of membrane delivery to the forming phagosome. The RE has a tubular structure and delivers membranes to regions of the cell surface that are undergoing dramatic reorganization (van Ijzendoorn, 2006), such as nascent phagosomes.

The initial impetus behind this study was to resolve a seeming discrepancy in the requirement for Cdc42 during integrin-mediated phagocytosis. Cdc42 inactivation appears not to affect integrin-mediated uptake of bacteria (Alrutz et al., 2001), whereas others found that Cdc42 inactivation negatively affects the integrin-mediated uptake of large (4 µm—larger than average bacteria) beads (Wiedemann et al., 2001). This discrepancy led us to hypothesize that Cdc42 dependence during uptake is governed by the size of the phagocytic particle. Accordingly, we found that although Cdc42-depleted cells internalized small particles efficiently, large particle uptake was defective. An intriguing and unique link between Cdc42 and the secretory machinery was then uncovered, leading to the discovery of the interaction between Cdc42 and the exocyst complex during phagosome formation.

Results

Impaired Cdc42 signaling leads to a selective defect in large particle uptake

Previous results indicated that integrin-promoted uptake of *Y. pseudotuberculosis* (1–2 µm in size) required active Rac1 but was unaffected by interfering forms of Cdc42 (Alrutz et al., 2001). Conflicting results indicate that Cdc42 is indeed required for uptake of 4-µm invasin-coated beads (Wiedemann et al., 2001). Also, in conflict with the bacterial uptake data is the observation that cell spreading on fibronectin, a ligand that engages many of the same integrin receptors as invasin, has been shown to require Cdc42 (Price et al., 1998). As cell spreading could equate to the phagocytosis of an infinitely large particle, one explanation for these results is that Cdc42 is only required for integrin-dependent processes that involve surface areas larger than *Y. pseudotuberculosis*. Alternatively, these results could be explained by invasin and fibronectin engaging integrins in different ways.

To analyze the role of Cdc42 in integrin-mediated processes, cell spreading on invasin-coated surfaces was characterized after RNAi inactivation. Cells were transfected with plasmids encoding shRNAs, which efficiently reduced Cdc42 protein levels as compared with scrambled shRNA (shScr) controls (Fig. S1 A). The depleted cells were replated on invasin-coated coverslips, and the extent of cell spreading was followed by live phase-contrast microscopy. Cdc42-depleted cells displayed a severe kinetic defect in spreading when compared with control cells, with almost no spreading taking place over 30 min (Fig. 1, A and B; and Video 1). This is consistent with data on spreading on fibronectin and argues that the absence of a requirement for Cdc42 in invasin-promoted processes is not because invasin engagement of integrins has special features not found in other integrin–ligand interactions.

To test the model that particle size determines Cdc42 requirement, control and Cdc42-depleted cells were challenged with particles of varying sizes coated with two different ligands. *Y. pseudotuberculosis* (~1–2 µm) were used to represent small phagocytic particles, whereas 2.9- and 4.5-µm beads coated with purified invasin were used as medium and large particles, respectively. Consistent with previous results using interfering forms of Cdc42 (Alrutz et al., 2001), depletion of Cdc42 had no effect on the uptake of *Y. pseudotuberculosis* and caused only a small depression in the uptake of 2.9-µm beads (Fig. 1 C). In contrast, depletion of Cdc42 resulted in a strong uptake defect for large particles (4.5-µm beads; Fig. 1 C). The size-dependent reduction was specific to Cdc42 depletion, as Rac1 depletion reduced the uptake efficiency of all tested particle sizes (Fig. 1 C). Strikingly, the size-dependent uptake defect in Cdc42-depleted cells was not limited to integrin-mediated uptake. Cdc42-depleted cells, expressing FcγRIIA and challenged with IgG-coated beads, also displayed a size-dependent uptake defect (Fig. 1 D), indicating that this phenomenon is widespread among receptor–ligand pairs.

Previous results indicated that integrin-promoted uptake was independent of NWASP (Alrutz et al., 2001), one of the key downstream effectors of Cdc42 that stimulates Arp2/3 complex function and actin rearrangement (Symons et al., 1996). To determine whether NWASP deficiency also leads to a size-dependent uptake defect, $NWASP^{-/-}$ mouse embryonic fibroblasts (MEFs) were challenged with invasin-coated small and large particles. Control experiments demonstrated that 1.5-µm invasin-coated beads behaved similarly to *Y. pseudotuberculosis* during uptake (unpublished data), thus 1.5-µm beads were used to represent small particles. Uptake of 4.5-µm beads by $NWASP^{-/-}$ cells was defective, whereas no such defect was observed with 1.5-µm beads (Fig. 1 E). Rac1 mediates actin remodeling through the activation of WASP family Verprolin-homologous family proteins in a manner similar

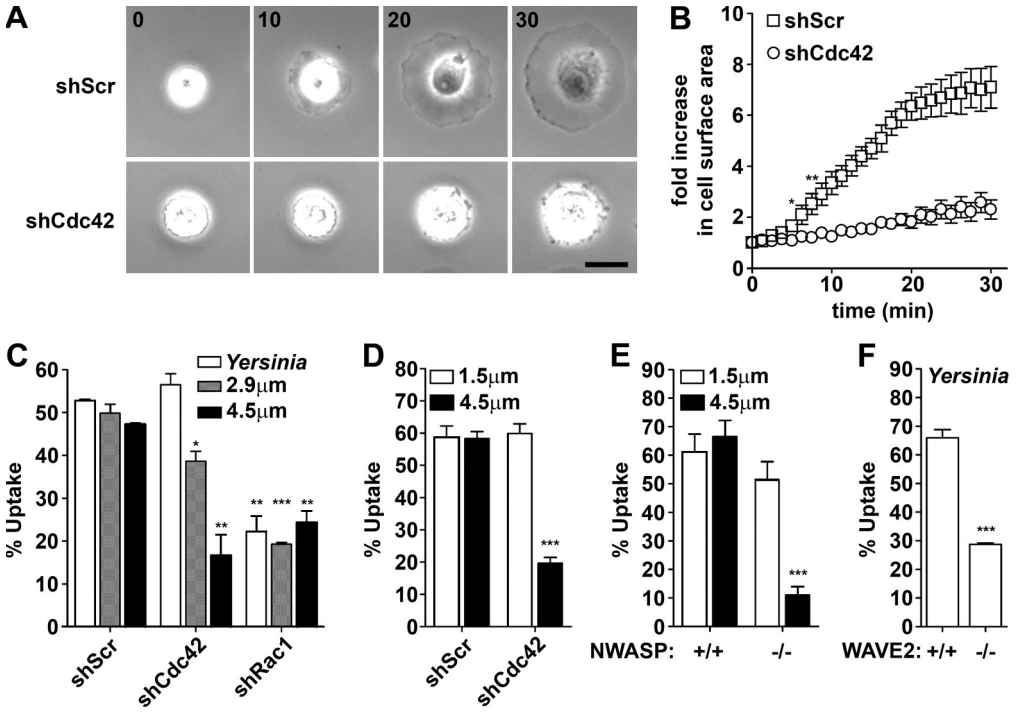

Figure 1. **Defects in Cdc42 signaling result in a size-dependent uptake defect.** (A) Cdc42 depletion leads to a kinetic defect in cell spreading on invasin. Control (shScr)- and Cdc42 (shCdc42)-depleted COS1 cells were plated onto invasin-coated glass coverslips, and spreading was visualized by phase-contrast time-lapse imaging. Numbers indicate time (in minutes). Bar, 10 µm. (B) Quantification of A. The area occupied by the cell was measured at each time point. Data are presented as fold increase in area, normalized to time = 0. (C) Cdc42-depleted cells internalize small particles but fail to internalize large particles efficiently. Control, Cdc42-depleted, and Rac1 (Rac1 shRNA [shRac1])-depleted COS1 cells were incubated with small (*Y. pseudotuberculosis*), medium (2.9-µm beads), or large (4.5-µm beads) invasin-coated particles. Uptake was then quantified microscopically. (D) FcR-mediated uptake in Cdc42-depleted cells is size dependent. Small (1.5 µm) or large (4.5 µm) IgG-coated beads were incubated with control or Cdc42-depleted COS1 cells expressing FcγRIIA, and uptake was quantified microscopically. (E) NWASP is required for the internalization of large particles but not for small particle uptake. NWASP$^{+/+}$ and NWASP$^{-/-}$ MEFs were incubated with 4.5- and 1.5-µm particles, and uptake was quantified microscopically. (F) WAVE2 is required for internalization of small particles. WAVE2$^{+/+}$ and WAVE2$^{-/-}$ MEFs were incubated with *Y. pseudotuberculosis*, and uptake was quantified microscopically. Error bars represent SEM. *, $P < 0.05$; **, $P < 0.01$; ***, $P < 0.001$.

to NWASP (Eden et al., 2002). In contrast to NWASP$^{-/-}$ cells, WAVE2$^{-/-}$ MEFs were defective for the uptake of small particles (Fig. 1 F), indicating that only the downstream effector of Cdc42 displays a size-dependent phenotype in this process, similar to the contrast between the roles of Rac1 and Cdc42 in uptake.

Rac1 activity can be influenced by the level and activation state of Cdc42 (Nobes and Hall, 1995; Price et al., 1998), so the size-dependent uptake defect observed in Cdc42-depleted cells may be caused by a selective reduction in Rac1 activity. By this model, the Cdc42 requirement would reflect a need for increased amounts of active Rac1 during large particle uptake relative to small particles. Therefore, fluorescence resonance energy transfer (FRET) microscopy was used to quantify Rac1 activation levels at nascent phagosomes in control and Cdc42-depleted cells (Fig. 2, A and B). Rac1 was found to be activated to the same level regardless of particle size or Cdc42 level (Fig. 2, C and D), indicating that Rac1 activity is not altered by a reduction in Cdc42 levels in this phagocytic system and that the cause of Cdc42 dependence lies elsewhere.

Another possibility for the observed differential requirement for Cdc42 is that receptor engagement by small particles leads to less Cdc42 activation than large particle engagement. To investigate this possibility, a ratiometric imaging method, measuring the interaction between activated endogenous Cdc42 and the Cdc42-binding domain (CBD) of WASP (Beemiller et al., 2010) was used. Both small and large particles were found to activate Cdc42 (Fig. S2 and Videos 2 and 3), similar to previous observations with FcR-mediated uptake (Beemiller et al., 2010), indicating that size dependence is not caused by variations in Cdc42 activation.

The size-dependent uptake defect in Cdc42-depleted cells could be caused by differences in the surface area between small and large particles. If so, increasing the total surface area of small phagocytic particles encountered by a cell should recapitulate the uptake defect. To address this possibility, uptake of small and large particles by the same cell was assessed in control and Cdc42-depleted cells (Fig. 3, A and E). Differing quantities of small particles were added so that the surface area ratio of small to large particles was low (Fig. 3, A–D) or similar (Fig. 3, E–H). Interestingly, even when the total small particle surface area was similar to the total large particle surface area, identical results were obtained regarding size dependence and Cdc42 requirement (Fig. 3 F). Small particles were internalized efficiently regardless of total surface area and Cdc42 depletion status. Notably, the same Cdc42-depleted cell that failed to internalize large particles efficiently internalized large numbers of small particles, indicating that

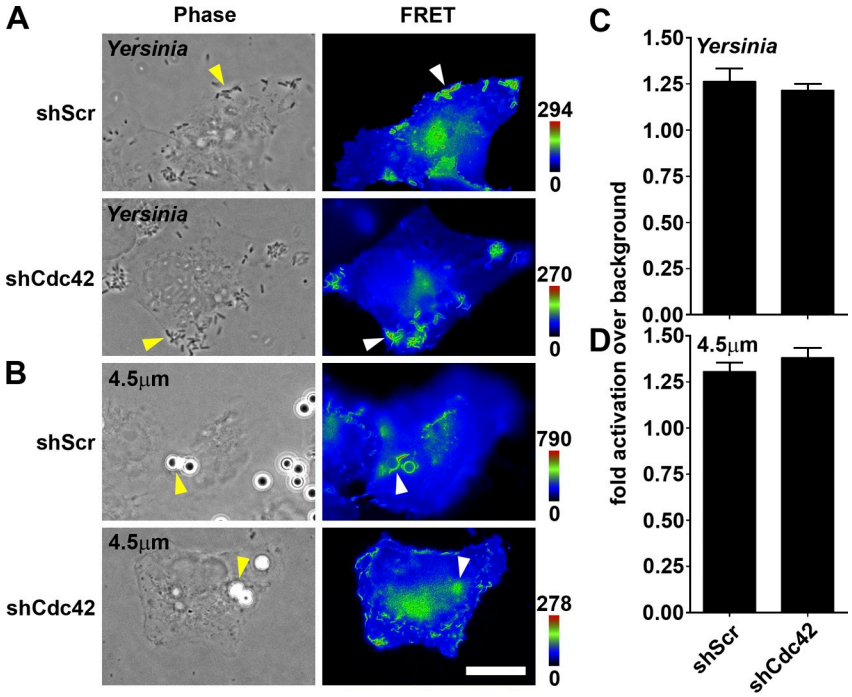

Figure 2. **Cdc42 depletion does not affect Rac1 activation levels at nascent phagosomes.** (A and B) Rac1 activity at the site of particle binding is not affected by Cdc42 depletion. Control (shScr) and Cdc42 (shCdc42)-depleted COS1 cells, expressing mCFP-Rac1 and PBD-mYFP were incubated with *Y. pseudotuberculosis* or 4.5-µm invasin-coated beads. Each condition was imaged microscopically for FRET analysis. Arrowheads denote regions of particle binding. Bar, 20 µm. (C and D) Quantification of A and B. The FRET signal at the site of particle attachment was quantified for each scenario. Error bars represent SEM.

each phagosome forms independently and that the molecular requirements for internalization are distinct for large and small particles.

Defects in Cdc42 signaling interfere with membrane flow

A series of experiments were performed to determine reasons for the size-dependent requirement for Cdc42. First, phagosome morphology in the presence and absence of Cdc42 was analyzed. To visualize nascent phagosome structure, a membrane-targeted GFP carrying the myristoylation site of Lyn kinase (referred to as Lyn-GFP) was used (Teruel et al., 1999). Control and Cdc42-depleted cells expressing Lyn-GFP were challenged with small and large particles, and phagosome formation was visualized by time-lapse microscopy. Membrane morphology during small particle (*Y. pseudotuberculosis*) uptake was unaffected by Cdc42 levels. Control and Cdc42-depleted cells internalized *Y. pseudotuberculosis* with relatively little membrane perturbation (Fig. 4, A and B; and Videos 4 and 5). Uptake of 4.5-µm beads by control depleted cells, however, stimulated a great deal of membrane perturbation (Fig. 4 C, 2 and 3 min images; and Video 6). A large degree of flux in GFP signal was

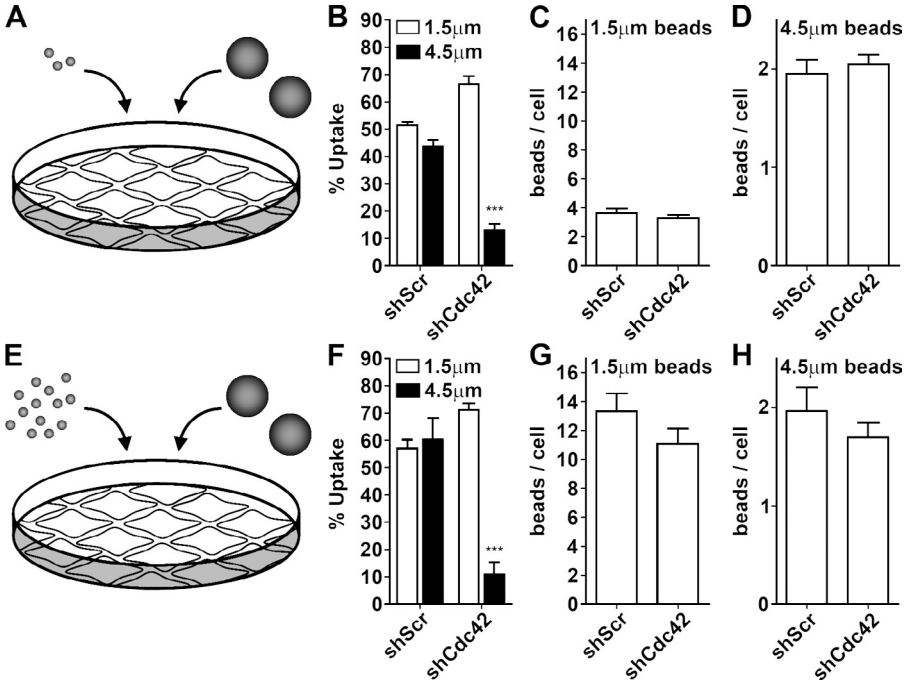

Figure 3. **Variations in phagocytic particle surface area do not affect uptake efficiency.** (A and E) The effects of varying small particle surface area upon uptake efficiency were quantified after coincubating cells with small and large particles. (A–H) Control (shScr) and Cdc42 (shCdc42)-depleted COS1 cells were challenged with a fixed MOI and 4.5-µm beads simultaneously, with 1.5-µm beads at low (A–D) or high (E–H) multiplicity, and uptake by the same cell of the two differently sized particles was quantified microscopically on a per-cell basis. The total number of small (C and G) and large (D and H) beads associated with each cell was used to determine multiplicity empirically. In the low multiplicity scenario (A–D), the large/small surface area ratio was ~5, and in the high multiplicity scenario (E–H), the large/small surface area ratio was ~1.3. Error bars represent SEM. ***, $P < 0.001$.

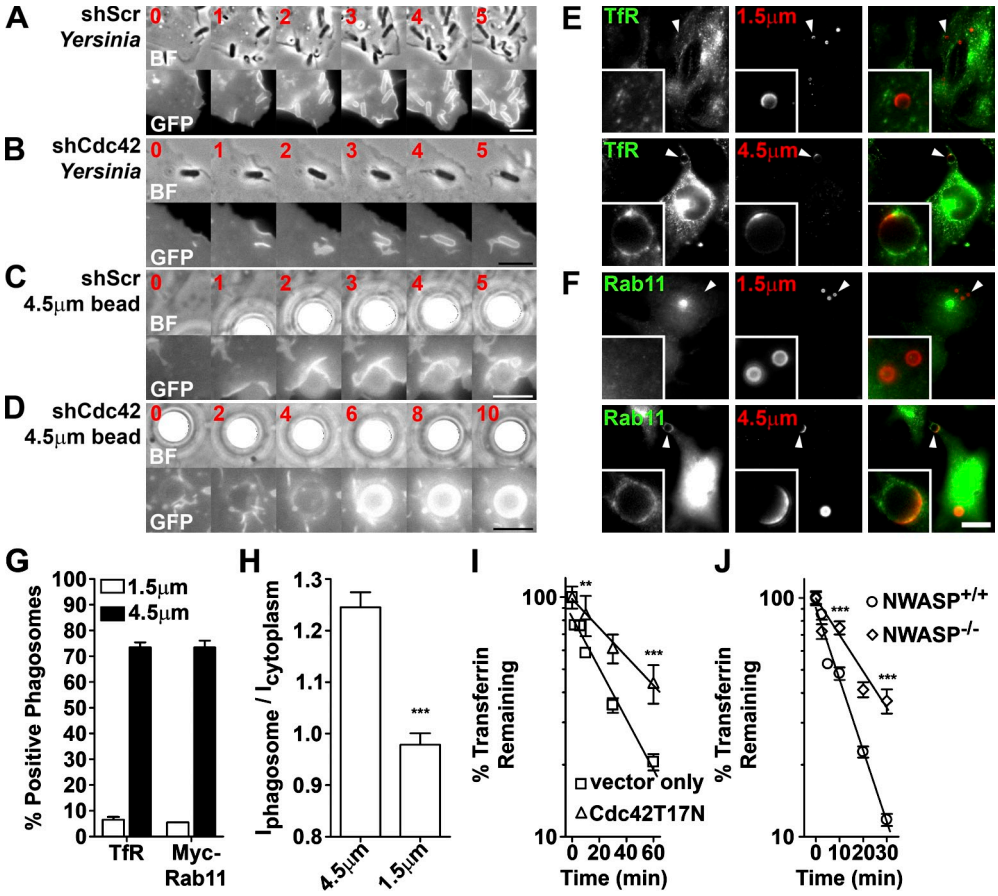

Figure 4. **Reduced membrane perturbation at the nascent phagosome in Cdc42-depleted cells.** (A–D) Characterizing phagosome morphology using time-lapse microscopy. *Y. pseudotuberculosis* or 4.5-μm beads were added to control (shScr) or Cdc42 (shCdc42)-depleted COS1 cells expressing Lyn-GFP and imaged every 15–20 s. At each time point, a bright-field and a GFP image were collected. Numbers indicate time (in minutes). Bars, 5 μm. (E) Transferrin receptor (TfR) localizes to large nascent phagosomes. COS1 cells were challenged with 1.5 (top)- and 4.5 (bottom)-μm beads and fixed, and endogenous TfR was detected using an anti-TfR antibody. In merged images, extracellular particles and TfR are pseudocolored red and green, respectively. Arrowheads point to phagosomes magnified in insets to emphasize the localization pattern. (F) Rab11 localizes to large nascent phagosomes. COS1 cells expressing Myc-Rab11 were challenged with 1.5 (top)- and 4.5 (bottom)-μm beads, and Myc-Rab11 was detected using an anti-Myc antibody. Bar, 10 μm; applies to E also. (G) Quantification of E and F. At least 50 phagosomes per condition were scored by eye for TfR or Rab11 recruitment. (H) The extent of TfR recruitment to phagosomes was determined by immunostaining for TfR and quantifying mean pixel intensity for ≥20 small and large phagosomes ($I_{phagosome}$). TfR staining at a nearby cytosolic region, devoid of attached particles, was determined also ($I_{cytoplasm}$). Extent of recruitment is presented as the quantity $I_{phagosome}/I_{cytoplasm}$. (I and J) Inactivation of Cdc42 or NWASP leads to reduced transferrin efflux. COS1 cells expressing dominant-negative Cdc42 and control cells (I) and NWASP$^{+/+}$ and NWASP$^{-/-}$ MEFs (J) were pulsed with fluorescent transferrin and chased in its absence. Remaining transferrin amounts were quantified microscopically. Error bars represent SEM. **, P < 0.01; ***, P < 0.001.

observed shortly after encounter with the large particle, which subsided as the particle was internalized. This was in dramatic contrast to Cdc42-depleted cells, which displayed very little membrane perturbation in response to large particle binding (Fig. 4 D and Video 7). It is unlikely that differences between control and Cdc42-depleted cells are caused by variations in the rate of actin polymerization because F-actin levels remain unchanged after Cdc42 depletion (unpublished data). These results are consistent with Cdc42 playing a role in modulating membrane structure at the site of large particle uptake.

The localization of endocytic markers to nascent phagosomes was examined to determine whether the size of the phagocytic particle affects recruitment patterns. Two endocytic markers, transferrin receptor (TfR) and Rab11, have been found on nascent phagosomes during erythrocyte engulfment (Cox et al., 2000). Interestingly, although we found TfR and Rab11 on phagosomes of large particles, there was very little recruitment of these proteins to small phagosomes (Fig. 4, E–G). The extent of localization was further characterized by quantifying the TfR pixel intensity at individual nascent phagosomes. This analysis showed that, per unit surface area in contact with the particles, more TfR associated with large phagosomes than small phagosomes (Fig. 4 H). Additionally, confocal microscopy showed a punctate pattern of TfR localization around large nascent phagosomes (unpublished data), indicating potential sites for exocytic vesicle fusion on the nascent phagosome. Collectively, these data are consistent with large particles selectively using the cell's secretory functions during uptake.

To determine whether a connection exists between the requirement for Cdc42 and the presence of secretory markers, the influence of Cdc42 inactivation upon bulk membrane flow to the cell surface was examined using fluorescently tagged transferrin in the absence of phagocytic particles. Cells, pulsed with Alexa Fluor 488–conjugated transferrin were chased in media

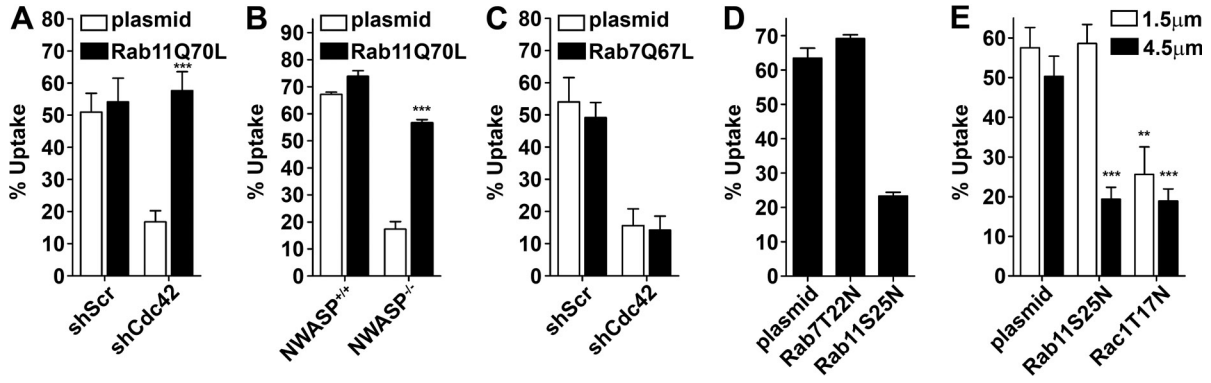

Figure 5. **Rab11 expression compensates for defective Cdc42 signaling during large particle internalization.** (A) Rab11 expression rescues large particle uptake defect in Cdc42-depleted cells. Control (shScr) and Cdc42 (shCdc42)-depleted COS1 cells were transfected with constitutively active Rab11 (Rab11Q70L) or a control plasmid and challenged with 4.5-µm beads. Uptake was quantified microscopically. (B) Rab11 expression rescues large particle uptake defect in NWASP$^{-/-}$ MEFs. NWASP$^{-/-}$ and NWASP$^{-/-}$ MEFs, expressing Rab11Q70L, were challenged with 4.5-µm beads, and uptake was quantified. (C) Rab7 expression does not rescue large particle uptake defect in Cdc42-depleted cells. Experiment performed as in A, using constitutively active Rab7 (Rab7Q67L). (D) Rab7 inactivation does not affect large particle uptake efficiency. COS1 cells were transfected with a control plasmid or a dominant-negative Rab7 (Rab7T22N) and challenged with 4.5-µm beads, and uptake was quantified. (E) Rab11 inactivation leads to a size-dependent uptake defect. COS1 cells were transfected with a control plasmid, dominant-negative Rab11 (rab11S25N), or dominant-negative Rac1 (Rac1T17N). Rac1T17N was included as a negative control. These cells were then challenged with 1.5- and 4.5-µm beads, and uptake was quantified. Error bars represent SEM. **, P < 0.01; ***, P < 0.001.

containing excess unlabeled transferrin and fixed at various time points, and the cell-associated fluorescence was quantified microscopically. The presence of an interfering form of Cdc42 caused a kinetic defect in transferrin efflux relative to the vector alone (Fig. 4 I), similar to previous work connecting Cdc42 with the secretory pathway (Kroschewski et al., 1999). Similar results were obtained using NWASP$^{-/-}$ MEFs when compared with NWASP$^{+/+}$ MEFs (Fig. 4 J), indicating that at least one well-characterized Cdc42 effector is involved in this process. These data indicate that Cdc42 signaling influences the rate of bulk membrane delivery to the cell surface.

Rab11 expression rescues the large particle uptake defect in Cdc42-depleted cells

Focal exocytosis of endomembranes has been implicated during phagosome formation (Bajno et al., 2000), so we postulated that decreased exocytic activity associated with Cdc42 inactivation (Fig. 4) could be responsible for defects in large particle uptake. This is supported by previous observations that Cdc42 acts as a regulator of endomembrane trafficking (Kroschewski et al., 1999; Garrett et al., 2000). Rab11 expression has been shown to affect the rate of membrane flow to the cell surface from the RE, as constitutively active Rab11 increases and dominant-negative Rab11 decreases this rate (Ren et al., 1998; Cox et al., 2000). To determine whether increased Rab11 activity could overcome the loss of Cdc42 function, control and Cdc42-depleted cells, expressing constitutively active Rab11 (Rab11Q70L), were challenged with 4.5-µm beads, and uptake efficiency was quantified. Expression of Rab11Q70L rescued the uptake defect in Cdc42-depleted cells but had no significant effect on the internalization efficiency of control depleted cells (Fig. 5 A). Rab11Q70L expression was also found to rescue the large particle uptake defect observed in NWASP$^{-/-}$ cells (Fig. 5 B). These data indicate that increasing membrane flow to the cell surface is sufficient to overcome uptake defects observed with both defective Cdc42 signaling and the loss of a downstream effector. Notably, this rescue was not a general feature of Rab protein expression. Rab7 is a GTPase required for late endosome maturation (Wang et al., 2011) and is not involved in membrane flow to the surface. We found that constitutively active Rab7 (Rab7Q67L) failed to rescue the large particle uptake defect in Cdc42-depleted cells (Fig. 5 C). Additionally, the efficiency of large particle internalization was unaffected by dominant-negative Rab7 (Rab7T22N) expression (Fig. 5 D).

The effect on phagocytosis of decreasing membrane flow to the cell surface was examined next. Expression of dominant-negative Rab11 in cells has been shown to slow trafficking to the cell surface (Zeng et al., 1999) and reduce the uptake efficiency of IgG-coated erythrocytes (Cox et al., 2000), so cells expressing dominant-negative Rab11 (Rab11S25N) were challenged with small and large particles. Expression of Rab11S25N led to a size-dependent uptake defect, similar to that observed in Cdc42-depleted cells (Fig. 5, D and E), consistent with a size-dependent requirement for membrane delivery to the cell surface. This defect in uptake was not caused by changes in steady-state levels of β1 integrin receptors on the plasma membrane. Flow cytometry showed that neither Cdc42 depletion nor the absence of NWASP reduced β1 integrin cell surface staining (unpublished data). Similarly, neither constitutively active nor dominant-negative Rab11 expression altered β1 integrin cell surface staining (unpublished data).

Because Rab11 expression could rescue the large particle uptake defect of Cdc42-depleted cells, the notion of a physical interaction between Cdc42 and Rab11 was examined. Cells expressing wild-type and two constitutively active forms of Cdc42 (Cdc42G12V and Cdc42F28L) along with wild-type Rab11 were lysed, and interaction between Cdc42 and Rab11 was assayed by immunoprecipitation and Western blotting. No interaction was observed, regardless of coimmunoprecipitation combination (Fig. S3 A).

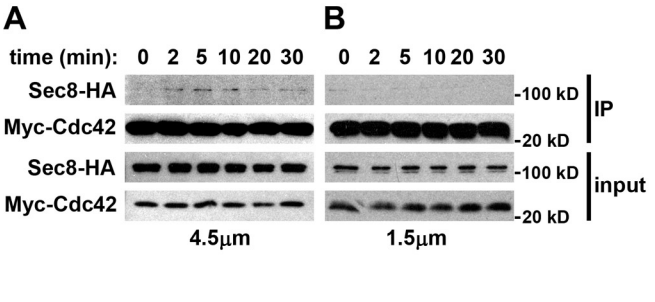

Figure 6. **Kinetic association of Cdc42 with the exocyst complex during large particle uptake.** (A and B) Sec8 associates with Cdc42 during large particle uptake. 293T cells were cotransfected with Myc-Cdc42wt, Sec8-HA, and Sec3-FLAG and were incubated with 4.5 (A)- or 1.5 (B)-μm beads. At the indicated times, cells were lysed, and Myc-Cdc42 was precipitated from the cleared lysates using anti-Myc antibody resin. Input and immunoprecipitate (IP) samples were analyzed by SDS-PAGE and Western blotting. (C) Quantification of A and B. Densitometry was performed on Western blots, and the quantity of Sec8-HA that precipitated with Myc-Cdc42 was normalized to input quantities and divided by starting amounts to derive the fold Sec8 immunoprecipitate. This assay was repeated multiple times, yielding similar results, and data are shown from one representative experiment.

Similarly, dominant-negative Rab11 did not interact with Cdc42 either (Fig. S3 B), whereas a known binding partner (CBD domain from WASP) coimmunoprecipitated with Cdc42 efficiently (Fig. S3 C). These results indicate that Cdc42 influences exocytic functions using binding partners other than Rab11.

Cdc42 interacts with the exocyst complex during large particle phagocytosis

An alternate site of interaction with the exocytic network could be proteins that act downstream of Rab11/RE. One potential target is the exocyst, a multicomponent complex involved in tethering post-Golgi vesicles to the plasma membrane (Munson and Novick, 2006), whose components were found in a proteomic analysis of *Drosophila melanogaster* phagosomes (Stuart et al., 2007). In mammalian cells, constitutively active Cdc42 interacts with the exocyst complex when two exocyst components associated with secretory vesicles, Sec8 and Sec3 (Sakurai-Yageta et al., 2008), are both expressed. However, there are no studies of wild-type Cdc42 associating with any exocyst components in response to an activation signal such as phagocytosis. Thus, to examine the possibility of Cdc42–exocyst interaction during phagocytosis, coimmunoprecipitation experiments were conducted using cells expressing wild-type Myc-Cdc42, Sec8-HA, and Sec3-FLAG. These cells were challenged with 4.5- and 1.5-μm beads, lysed at various time points, and Myc-Cdc42 immunoprecipitated, and the amount of coprecipitated Sec8-HA was determined using Western blotting. Remarkably, 4.5-μm beads stimulated a transient Cdc42/Sec8 association (Fig. 6, A and C). An increase in association was observed within 2 min after the addition of beads to cells, peaking at 5 min (Fig. 6 C). Association levels then diminished, reaching original levels at ∼15 min. This is in contrast to 1.5-μm beads, which showed no increase in Cdc42/Sec8 association throughout the experiment (Fig. 6, B and C). These data indicate that large particles selectively stimulate Cdc42 association with exocyst components.

The exocyst complex plays a functional role during large particle uptake

Because we found that Cdc42–exocyst interaction is stimulated by large particle uptake, the interplay between Cdc42 and the exocyst complex during phagocytosis was examined further. In addition to the interaction data discussed in Fig. 6, genetic evidence links Cdc42 and the exocyst complex: expression of "active" mutants of the exocyst subunit, Exo70, has been shown to rescue the temperature sensitivity of a *cdc42* mutant in *Saccharomyces cerevisiae* (Wu et al., 2010). Exo70 localizes to the plasma membrane through interaction with inner leaflet lipids and is thought to create docking sites for the rest of the exocyst complex, thereby demarcating the site of assembly (Liu et al., 2007). Because the expression of an active form of Exo70 can bypass the requirement for Cdc42 in yeast, we examined whether the expression of human Exo70 could rescue large particle uptake defects in the absence of Cdc42 function. Control and Cdc42-depleted cells, expressing Exo70, were challenged with 4.5-μm beads. Exo70 expression had no effect on uptake in control depleted cells (Fig. 7 A). In contrast, Exo70 expression in Cdc42-depleted cells increased uptake efficiency to levels indistinguishable from control samples (Fig. 7 A), suggesting that an increase in the number of tethered exocyst complexes at the plasma membrane could rescue the large particle uptake defect in the absence of Cdc42 signaling. Exo70 expression did not rescue defective uptake of large particles by Rac1-depleted cells (Fig. 7 B), indicating that the rescue was specific to the absence of Cdc42 and that Exo70 could not bypass a requirement for cytoskeletal rearrangements associated with Rac1 activity. Interestingly, Exo70 expression did not rescue defective uptake of large particles in NWASP$^{-/-}$ MEFs (Fig. 7 C).

To determine whether exocyst function is specifically required for uptake of large particles, the effect of reduced Exo70 activity on uptake of differently sized beads was examined. Endogenous Exo70 was depleted using synthetic RNAi-mediated knockdown (KD). Quantitative RT-PCR and Western analysis were used to monitor the extent of Exo70 depletion, and both mRNA and protein levels were found to be greatly reduced compared with the control (Fig. S1, B and C). Exo70-depleted cells did not internalize 4.5-μm beads efficiently (Fig. 7 D), whereas uptake of 1.5-μm beads was unaffected (Fig. 7 F), indicating that robust exocyst function is selectively required during large particle uptake. Intriguingly, Exo70 was also required for the FcR-mediated internalization of large particles (Fig. 7 E), whereas its depletion did not affect small particle uptake (Fig. 7 G). These data indicate that the requirement for exocyst function is not limited to β1 integrin–mediated uptake and is likely a general requirement for efficient phagocytosis.

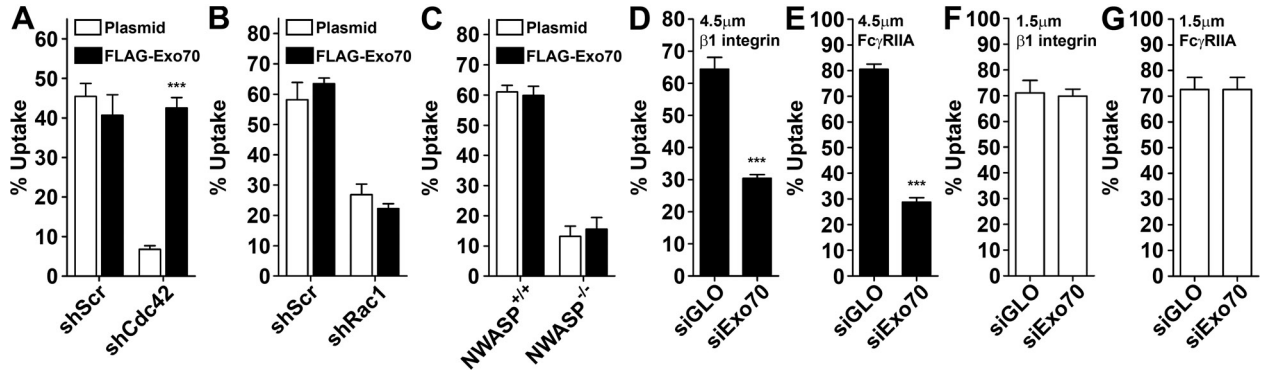

Figure 7. **Exocyst function is required for large particle uptake.** (A) Expression of Exo70 rescues large particle uptake defect in Cdc42-depleted cells. Control (shScr) and Cdc42 (shCdc42)-depleted COS1 cells were transfected with FLAG-Exo70 or a control plasmid and challenged with 4.5-µm beads. Uptake was quantified microscopically. (B) Exo70 expression does not rescue large particle uptake defect in Rac1-depleted cells. Control and Rac1 (Rac1 shRNA [shRac1])-depleted COS1 cells, expressing FLAG-Exo70, were challenged with 4.5-µm beads, and uptake was quantified. (C) Large particle uptake defect in NWASP$^{-/-}$ cells is not rescued by Exo70 expression. NWASP$^{+/+}$ and NWASP$^{-/-}$ cells were transfected with FLAG-Exo70 or a control plasmid and challenged with 4.5-µm beads. Uptake was quantified microscopically. (D and E) Exo70 depletion leads to defective large particle uptake. Control (siGLO) and Exo70 (siExo70)-depleted HeLa cells (D) or FcγRIIA-expressing HeLa cells (E) were challenged with invasin-coated (D) or IgG-coated (E) 4.5-µm beads, and uptake was quantified microscopically. (F and G) Exo70 depletion does not interfere with internalization of small particles. Control (siGLO) and Exo70 (siExo70)-depleted HeLa cells (F) or FcγRIIA-expressing HeLa cells (G) were challenged with invasin-coated (D) or IgG-coated (E) 1.5-µm beads, and uptake was quantified microscopically. Error bars represent SEM. ***, $P < 0.001$.

As there was a transient Cdc42–exocyst interaction during large particle uptake (Fig. 6) and because Exo70 depletion interfered with uptake of large particles (Fig. 7), we decided to test whether Exo70 stabilizes the interaction between Cdc42 and the exocyst complex. Coimmunoprecipitation could not demonstrate stable Cdc42–Exo70 interaction in cells expressing constitutively active Cdc42 and wild-type Exo70 (unpublished data). It is possible that the Cdc42 interaction with an Exo70-containing complex is transient or that Exo70 plays a role in stabilizing a complex that allows Cdc42 to recognize other exocyst components. Therefore, we investigated whether the interaction of Cdc42 with the exocyst complex required the presence of Exo70. Using the strategy used in Fig. 6, we tested whether Exo70 was required for Cdc42 interaction with a Sec8/Sec3-containing complex. Coimmunoprecipitation of constitutively active Myc-Cdc42 (Cdc42V12), Sec8-HA, and Sec3-FLAG was tested in control and Exo70-depleted cells and analyzed by Western blotting. Interestingly, Exo70 depletion clearly reduced the efficiency of Sec8 and Sec3 coassociation with Cdc42 (Fig. 8 A, quantified on the right). These results indicate that Exo70 is required for high efficiency interaction between Cdc42 and Sec3/Sec8 and is indeed necessary for maintaining the integrity of the interaction complex.

The interplay between Exo70 and Rab11 during large particle uptake was examined next to examine the likely order that these two proteins function during uptake. A recent study has shown that the depletion of either Rab11 or Exo70 stalls cargo delivery at the plasma membrane, which indicates that both proteins are intimately involved in the tethering of vesicles to the plasma membrane (Takahashi et al., 2012). We show that the inactivation of either Rab11 or Exo70 inhibited large particle uptake (Figs. 5 and 7, respectively), but the molecular sequence of action between these two proteins during uptake is unknown. Two experiments were performed to examine the epistatic relationship between Rab11 and Exo70 during phagocytosis. First, the effect of exogenous Exo70 expression in the presence of an interfering form of Rab11 was examined. We observed that Exo70 expression almost completely rescued the defect in uptake resulting from the expression of dominant-negative Rab11 (Fig. 8 B). Next, we quantified uptake in Exo70-depleted cells, expressing constitutively active Rab11, to determine whether Rab11 activity could bypass a requirement for Exo70. In contrast to the observation that Exo70 expression could rescue the uptake defect in the absence of Rab11 activity, depletion of Exo70 could not be bypassed by constitutively active Rab11 expression (Fig. 8 C). These data are consistent with the model that Exo70 acts downstream of Rab11, demonstrating a critical role for the exocyst complex during phagosome formation.

Discussion

Rho family GTPases have long been known to be important regulators of particle uptake, and their central role in the process has been presumed to involve coordination of critical cytoskeletal rearrangements involved in phagosome closure (Niedergang and Chavrier, 2005). In this work, we demonstrate that Cdc42 is important for membrane delivery to the phagosome, thereby establishing a connection between the cytoskeletal and secretory networks during phagocytosis. Data presented here point to a model in which size governs the Cdc42-mediated requirement for exocytosis during phagosome formation. In contrast to small particles, large particles were associated with the recruitment of the exocytic machinery (Fig. 4) and stimulated the temporal association of the exocyst complex with Cdc42 (Fig. 6). Additionally, only large particles required the exocytic proteins Rab11 and Exo70 for uptake (Figs. 5 and 7), demonstrating a functional role for the exocyst complex during receptor-mediated uptake that was previously uncharacterized.

In this work, we show several functional similarities between integrin- and FcR-mediated uptake. We show that uptake in the absence of Cdc42 is size dependent in both cases (Fig. 1), that Cdc42 activation kinetics during uptake are similar

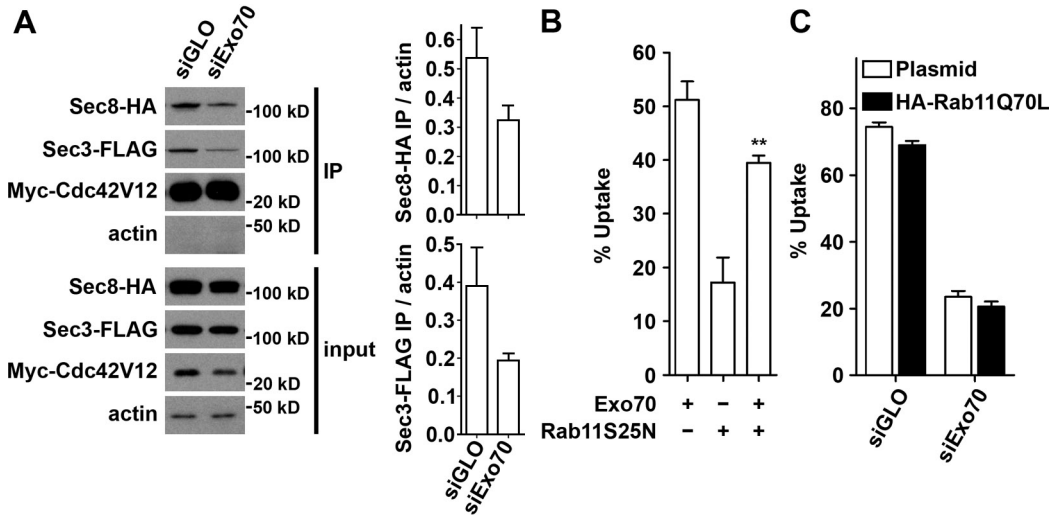

Figure 8. **Exo70 interaction with the exocyst complex and Rab11 during phagosome formation.** (A) Cdc42–exocyst association requires Exo70. Control (siGLO) and Exo70 (siExo70)-depleted 293T cells were transfected with constitutively active Cdc42 (Myc-Cdc42V12), Sec8-HA, and Sec3-FLAG. Cells were lysed, and Myc-Cdc42 was precipitated from the cleared lysates using anti-Myc antibody resin. Input and immunoprecipitate (IP) samples were analyzed by SDS-PAGE and Western blotting. Densitometry was used to quantify the amount of Sec8 or Sec3 that precipitated with Myc-Cdc42, which was then normalized to input quantities. (B) Exo70 expression rescues large particle uptake defect in the absence of Rab11 activity. HeLa cells expressing either Exo70 or dominant-negative Rab11 (Rab11S25N) or both were challenged with 4.5-µm beads, and uptake was quantified microscopically. (C) Control (siGLO) or Exo70 (siExo70)-depleted HeLa cells were transfected with an empty plasmid or constitutively active Rab11 (HA-Rab11Q70L) and challenged with 4.5-µm beads. Uptake was quantified microscopically. Error bars represent SEM. **, $P < 0.01$.

(Fig. S2; Beemiller et al., 2010), and that both processes require exocyst function (Fig. 7). Collectively, these data indicate that the molecular requirements for particle internalization are largely independent of cell type and receptor–ligand combinations and that size dependence and a requirement for efficient exocytic activity are general features of phagocytic systems.

We showed that large particle uptake defect in NWASP$^{-/-}$ cells could be rescued by Rab11 expression (Fig. 5) but not with Exo70 (Fig. 7). This dichotomy implies that the mode of rescue is different for the two molecules. Exo70 is thought to act as a docking and assembly site for the exocyst complex (Liu et al., 2007), and its exogenous expression likely increases the number of functional exocyst complexes in the cell. Rescue in Cdc42-depleted cells could come from the combination of residual Cdc42 levels that stimulate low level NWASP activity, which in combination with Exo70 lead to increased uptake. Exogenous expression of Rab11 has been shown to increase the rate of trafficking to the plasma membrane (Ren et al., 1998; Cox et al., 2000), so rescue by Rab11 expression is most likely caused by a general increase in membrane trafficking. Increasing exocyst assembly sites through Exo70 expression without a large-scale increase in membrane flow could be sufficient for rescuing the RNAi-mediated depletion of Cdc42 but is not sufficient for rescuing the genetic absence of NWASP. However, the increase in membrane flow caused by Rab11 expression may be sufficiently robust for rescuing uptake in both Cdc42-depleted and NWASP$^{-/-}$ cells.

The precise role of NWASP in the context of membrane exocytosis is unknown. We show that although both Cdc42 and NWASP are required for large particle uptake (Fig. 1), the absence of NWASP could not be rescued by the exogenous expression of Exo70 (Fig. 7). This phenomenon could be described by several possibilities. NWASP may be involved in the uptake process in a fashion that is independent of the exocyst complex. Alternatively, NWASP signaling could be occurring in a Cdc42-independent manner, which has been observed previously (Rohatgi et al., 2001). Although no direct role for NWASP has been described during exocytosis, WASP-like proteins have been implicated in vesicle delivery to the plasma membrane (Kim et al., 2007), and the interaction of exocyst components and actin nucleation–promoting factors, such as NWASP, has been the subject of recent investigations (Liu et al., 2012).

Although we have shown that Exo70 is required for Cdc42–exocyst interaction (Fig. 8), the precise nature of the complex is unclear. In yeast, Cdc42 interacts with the N terminus of the Sec3 component of the exocyst complex (Zhang et al., 2001), but the N-terminal sequence and subcellular localization patterns for yeast and mammalian Sec3 differ (Matern et al., 2001). Thus, Cdc42 and Sec3 may not interact in mammalian systems. Several small GTPases have been shown to interact with exocyst components in mammalian systems, namely Sec5, Sec10, Sec15, and Exo70 (Sugihara et al., 2002; Inoue et al., 2003; Prigent et al., 2003; Zhang et al., 2004; Zuo et al., 2011), and Cdc42 could potentially interact with these subunits during uptake.

To examine the nature of the exocyst localization during phagosome formation more closely, we constructed fluorescently tagged versions of each exocyst complex member and studied recruitment patterns to the nascent phagosome (Fig. S5). Exo70 was efficiently recruited to large phagosomes, whereas Sec5 and Sec15 showed weaker levels of localization. This finding is in contrast to previous work showing that most exocyst components (all except Sec6 and Exo84) are found on nascent phagosomes (Stuart et al., 2007). As most of the exocyst components, when expressed as fluorescently tagged fusions, showed diffuse cytoplasmic localization (Fig. S5 B), concentration at the nascent phagosome was not readily detected. Previous work using purified

phagosomes and mass spectrometry (Stuart et al., 2007) was able to overcome this problem by isolation from cytoplasmic contamination. Given the lack of clear concentration of exocyst components about the membrane and the fact that we could not detect interaction between Cdc42 and Exo70 by coimmunoprecipitation (unpublished data), we believe that exocyst complex formation during phagocytosis is transient and highly susceptible to perturbations, such as component depletion or exogenous expression of individual components.

The small GTPase RalA has been implicated in exocyst complex assembly and stability (van Dam and Robinson, 2006) and has been shown to mediate the formation of Cdc42-dependent structures such as filopodia (Sugihara et al., 2002) and *S. enterica* invasion foci (Nichols and Casanova, 2010). However, we found that RalA inactivation does not affect integrin-mediated uptake efficiency and that RalA is not activated during large particle phagocytosis (Fig. S4), indicating that RalA is not playing a role in the processes described in this work. Processes such as ciliogenesis (Das and Guo, 2011) that require constitutive exocytosis do not appear to need Ral function, and although no Ral homologue is found in the budding yeast *S. cerevisiae* (Lipschutz and Mostov, 2002), the exocyst assembles and functions stably (TerBush et al., 1996). It is possible that the regulatory proteins described in this work, namely Rab11 and Cdc42, modulate critical exocytic events without contribution from RalA.

Our data suggest that small particles are internalized quietly from a signaling standpoint: few changes in membrane morphology at the site of attachment (Fig. 4) are accompanied by a brief peak of Cdc42 activity that subsides quickly (Fig. S2) with no requirement for membrane delivery from internal sources (Figs. 5–7). The quiet nature of small particle entry could be advantageous to invading particles, such as intracellular bacterial pathogens. The bacterial pathogen could be stimulating few enough pathways to be phagocytosed but escape immune detection during the entry process, which may be deleterious to the invading pathogen.

Phagocytic uptake of apoptotic bodies shares several key characteristics with the large particle phagocytic system tested here in our study: apoptotic cells are internalized by zippering phagocytosis (Krysko et al., 2006), they are internalized by binding to integrin receptors (Savill et al., 2002), among others, and internalization of apoptotic cells requires both Cdc42 and WASP (Leverrier and Ridley, 2001; Leverrier et al., 2001). Thus, it is tempting to compare the implications of our observed defects in large particle uptake to defects in apoptotic cell clearance. Several autoimmune diseases are associated with impaired clearance of dead cells (Nagata, 2007). Thus, impairments in signaling that lead to defects in apoptotic cell phagocytosis, such as defects in Cdc42, Rab11, or Exo70 function described in our work, may potentially contribute to the development of autoimmunity.

In this work, we have demonstrated that the size of the phagocytic particle is a critical determinant of signaling potential during uptake. We have established a molecular link between the cytoskeletal and the exocytic machineries that was previously unknown. Additionally, we have established a functional role for the exocyst complex during receptor-mediated uptake.

Materials and methods

Cell culture and transfection

COS1, HeLa, and 293T cells (obtained from American Type Culture Collection) and NWASP$^{-/-}$ and WAVE2$^{-/-}$ MEFs (gifts from S. Snapper, Massachusetts General Hospital, Boston, MA) were maintained in DMEM supplemented with 10% heat-inactivated fetal bovine serum. Cells were transfected using Lipofectamine 2000 (Invitrogen) or FuGENE HD (Roche) per the manufacturers' recommendations. Typically, cells were analyzed 16–20 h after transfection, except for RNAi transfections, which were performed for 40–48 h. All plasmids used in this study are listed in Table S1.

RNAi KD

Cdc42 and Rac1 were depleted using plasmids encoding shRNAs. For these experiments, a new plasmid based on pRNAT-U6.1/neomycin (GenScript) was constructed that encodes mCherry (Shaner et al., 2004), whose expression could be used a proxy for protein depletion. shRNA sequences used are as follows: scrambled KD, 5′-AATTCTCCGAACGTGTCACGT-3′; Cdc42 KD, 5′-AAGTGGGTGCCTGAGATAACT-3′ (Wilkinson et al., 2005); and Rac1 KD, 5′-AAGGAGATTGGTGCTGTAAAA-3′ (Chan et al., 2005). The extent of KD was examined by Western blotting using monoclonal anti-Cdc42, anti-Rac1 (both obtained from BD), and antitubulin (Sigma-Aldrich) to control for loading (Fig. S1). Exo70 was depleted using a synthetic duplex RNA (Thermo Fisher Scientific) with the following sequence: 5′-GGUUAAAGGUGACUGAUUAUU-3′ (Zuo et al., 2006). Efficiency of Exo70 depletion was examined using quantitative real-time PCR and Western blotting with an anti-Exo70 antibody (Abcam).

Microscopy

All live-cell imaging was performed on a wide-field microscope (Axiovert 200M; Carl Zeiss) using a 10×, NA 0.3 Plan Neofluar or a 63×, NA 1.4 Plan Apochromat lens. The microscope was equipped with an environmental control chamber, standard FITC, TRITC, and DAPI filter cube sets (Chroma Technology Corp.), and a charge-coupled device camera (C4742-95-12ERG; Hamamatsu Photonics), all controlled by the Openlab imaging software package (PerkinElmer).

Fixed samples (FRET experiments and all quantitative uptake assays) were analyzed on a wide-field microscope (TE300; Nikon) equipped with 60×, NA 1.4 Plan Apochromat and 100×, NA 1.3 Plan Fluor lenses, standard YFP, CFP, and YFP/CFP FRET filter cube sets (Chroma Technology Corp.), and a charge-coupled device camera (C4742-98-24NR; Hamamatsu Photonics), controlled by the IPLab/iVision software package (Scanalytics/BD).

All image analysis was performed using either Openlab or IPLab/iVision. Figures were assembled using Photoshop (Adobe).

Cell spreading on invasin

8-well chambered coverslips (LabTek) were coated with 5 µg/ml maltose-binding protein (MBP)-Inv497 (C-terminal 497 aa of invasin fused to MBP) in PBS overnight at 4°C. Control and Cdc42-depleted cells were lifted using PBS + 10 mM EDTA, plated onto the coated dishes by centrifugation, and moved immediately to the microscope with a heated stage and imaged using a 10× objective lens for 30 min at 15-s intervals. For quantification, the area occupied by each cell was manually delineated and measured using the Openlab software package. Number of image sequences used for quantification is as follows: shScr, $n = 5$; and shCdc42, $n = 9$.

Quantifying uptake efficiency

Bacterial uptake was quantified on a per-cell basis as previously described (Mohammadi and Isberg, 2009) using a virulence plasmid-deficient *Y. pseudotuberculosis* strain. In brief, overnight cultures of bacteria were diluted 1:40 into fresh media and grown to mid–exponential phase (optical density of ∼0.7). Bacteria were added to cells grown on coverslips at a multiplicity (MOI) of ∼10, and uptake was allowed to proceed for 20 min. Cells were then fixed, and uptake was quantified microscopically on a per-cell basis.

For experiments involving bead uptake, 1.5-, 2.9-, or 4.5-µm latex beads (Polysciences, Inc.) were incubated overnight at 4°C with 1.5, 0.75, or 0.5 mg/ml purified MBP-Inv497, respectively. Beads were washed and stored at 4°C until use. Coated beads were added to cells grown on coverslips (MOI of ∼5–10) and briefly centrifuged (2 min at 300 *g*). Uptake was allowed to proceed for 30 min. Cells were then fixed, and uptake efficiency was quantified microscopically on a per-cell basis. Anti-MBP antibodies (New England Biolabs, Inc.) were used to detect MBP-Inv497.

For antibody coating, 1.5- or 4.5-µm beads were coated with 1 or 3 mg/ml rabbit IgG (Sigma-Aldrich), respectively. Beads were then washed

and stored at 4°C until use. Cells were transfected with FcγRIIA overnight (gift from E. Caron, Imperial College, London, England, UK), and beads were added and centrifuged briefly as in the previous paragraph. Cells were fixed after 30 min, and uptake was quantified exactly as described for MBP-Inv497 beads except that particles were visualized using anti–rabbit fluorescent antibodies.

Rac1 FRET imaging

Cells expressing mCFP-Rac1wt and p21-binding domain (PBD)-mYFP were incubated with small or large particles for 20 min. Cells were then washed, fixed, and processed for imaging. Imaging and analysis were performed exactly as previously described (Wong and Isberg, 2005). In brief, CFP, YFP, and FRET images were captured for each sample, and regions of interest (ROIs) at each nascent phagosome (i.e., with partially internalized particles) and at cytosolic regions with no bound particles were selected. For each ROI, sensitized FRET values (sFRET), which are corrected for cross-excitation and bleed through, were calculated. Subsequently, FRET values that were normalized to the expression levels of the donor and acceptor (nFRET) were calculated using the following equation:

$$\text{nFRET} = \frac{\text{sFRET}}{\sqrt{I_{CFP} \times I_{YFP}}}.$$

I represents the mean intensity for the indicated fluorescence channel. The fold increase in Rac1 activation was calculated by dividing the phagosome nFRET value by the cytosolic nFRET value.

Ratiometric imaging

The kinetics of Cdc42 activation in response to small and large particles was quantified using ratiometric imaging, essentially as previously described (Beemiller et al., 2010). In brief, cells were transfected with mCitrine-CBD (gift from J. Swanson, University of Michigan Medical School, Ann Arbor, MI) and mCherry in 35-mm glass-bottom dishes (MatTek). Cells were serum starved for ≥3 h before the addition of phagocytic particles. Imaging commenced immediately after the addition of small or large particles. Cells were imaged every 20 s for 20–30 min. Phase-contrast, YFP, and RFP images were captured at each time point. Image analysis was performed essentially as described previously (Henry et al., 2004). Image sequences were synchronized to the frame at which a bead came in contact with the cell, and a circular ROI, covering the phagocytic particle, was drawn on the phase-contrast image. The mean intensity of this ROI was determined for the YFP and RFP images, and a ratio of YFP to RFP was calculated for each time point (termed Rp). Next, mean intensities for YFP and RFP were determined for the whole cell, and a ratio of YFP to RFP was calculated (Rc). Finally, a recruitment index was calculated for each phagosome at each time point by dividing Rp by Rc. The number of image sequences used for quantification is as follows: 1.5 µm mCitrine/mCherry, $n = 8$; 1.5 µm mCitrine-CBD/mCherry, $n = 13$; 4.5 µm mCitrine/mCherry, $n = 5$; and 4.5 µm mCitrine-CBD/mCherry, $n = 5$.

Time-lapse microscopy with Lyn-GFP

Cells were grown and transfected with Lyn-GFP (gift from T. Meyer, Stanford University School of Medicine, Stanford, CA) in 35-mm glass-bottom dishes. Cells were serum starved ∼3 h before imaging. Imaging was initiated right after phagocytic particles were added to dishes and proceeded for 20–30 min.

TfR and Rab11 staining

COS1 cells were incubated with coated 1.5- or 4.5-µm beads and fixed after 30 min. The extracellular portions of the phagocytic particles were stained using anti-MBP antibodies (New England Biolabs, Inc.). Cells were then permeabilized and incubated with the anti-TfR antibody (Invitrogen). Coverslips were washed, and images were captured microscopically. To visualize Rab11 localization to nascent phagosomes, COS1 cells expressing Myc-Rab11 were incubated with 1.5- and 4.5-µm beads and fixed. Extracellular particles were visualized using anti-MBP antibodies, and anti-Myc antibodies (Santa Cruz Biotechnology, Inc.) were used to detect Myc-Rab11. The mean percentage of phagosomes that displayed positive staining was graphed.

Quantifying transferrin efflux

COS1 cells or MEFs were serum starved in serum-free media (DMEM) and loaded with 20 µg/ml iron-loaded Alexa Fluor 488–conjugated transferrin (Invitrogen) for 1 h. Cells were washed (time = 0) and allowed to efflux transferrin in serum-free media supplemented with 100 µg/ml apotransferrin (Invitrogen) and 100 µM desferrioxamine (Sigma-Aldrich). At the indicated times, cells were fixed and imaged to quantify remaining transferrin amounts. The mean fluorescence at two ROIs per cell was determined, and ≥20 cells were analyzed per time point. Values were normalized to the mean fluorescence values at time = 0.

Cdc42–exocyst coimmunoprecipitation assay

293T cells, expressing Myc-Cdc42wt, Sec8-HA, and Sec3-FLAG, were serum starved for 3–4 h. They were then incubated with 1.5- or 4.5-µm beads (MOI of ∼1) for 0, 2, 5, 10, 20, and 30 min. At each time point, cells were lysed using 500 µl lysis buffer and collected by scraping with a rubber policeman. Lysates were cleared by centrifugation, and 20 µl was saved as input. 400 µl cleared lysate was incubated with 25 µl anti-Myc resin (Santa Cruz Biotechnology, Inc.) for 1 h at 4°C with agitation. Beads were then washed 3× in wash buffer (lysis buffer with 0.1% Triton X-100), resuspended in 50 µl sample buffer, and eluted by boiling for 5 min. 10 µl of these samples was loaded on SDS-PAGE gels; input samples were diluted 20-fold, and 10 µl was loaded. For experiments with Myc-Cdc42V12, no beads were added. Cells were treated exactly the same otherwise.

Rab11/Cdc42 coimmunoprecipitation assay

This experiment was performed essentially like the Cdc42–exocyst immunoprecipitation experiment described in the previous section. In brief, 293T cells, expressing Myc-Cdc42wt, G12V, or F28L (Lin et al., 1997) with HA-mYFP, HA-mYFP-Rab11wt, or HA-mYFP-Rab11S25N were lysed, and Cdc42 was precipitated using the anti-Myc antibody resin. Beads were then washed and eluted by boiling in sample buffer. Eluate (immunoprecipitation) and input samples were analyzed by Western blotting using anti-Myc and anti-HA antibodies (both obtained from Santa Cruz Biotechnology, Inc.).

RalA activation assay

293T cells were serum starved for 3–4 h and then incubated with 4.5-µm beads (MOI of ∼1) for 0, 2, 5, 10, 20, and 30 min. At each time point, 300 µl lysis buffer was added, and cells were collected by scraping with a rubber policeman. Lysates were cleared by centrifugation, and 20 µl was saved as input. 50 µl cleared lysate was incubated with 25 µl GST-Sec5RBD (Ral-binding domain of Sec5 fused to GST) beads (gift from R. Wong and L. Feig, Tufts University School of Medicine, Boston, MA) for 30 min at 4°C with agitation. Sec5RBD binds to endogenous RalA-GTP, allowing for the isolation of active RalA from the inactive. Beads were then washed 3× in wash buffer (same as lysis buffer except with 0.1% Triton X-100), resuspended in 50 µl sample buffer, and eluted by boiling for 5 min. 10 µl of these samples were loaded on SDS-PAGE gels; input samples were diluted 20-fold, and 10 µl was loaded. A monoclonal anti-RalA antibody (BD) was used to detect endogenous RalA.

Statistical analysis

Each assay presented here was performed at least three times. Unless otherwise indicated, graphs depict mean values ± SEM. Microscopic assays on fixed samples were performed in triplicate (three coverslips) and quantified by scoring 30–50 cells per coverslip. Images presented here are representative of each sample analyzed. Data were analyzed using Prism (GraphPad Software), and p-values were generated using a two-tailed unpaired *t* test: *, $P < 0.05$; **, $P < 0.01$; ***, $P < 0.001$.

Online supplemental material

Fig. S1 shows RNAi-mediated depletion of Cdc42, Rac1, and Exo70. Fig. S2 shows that Cdc42 is activated in response to small and large particles. Fig. S3 shows that coimmunoprecipitation experiments show no Cdc42 association with Rab11. Fig. S4 shows that RalA inactivation does not affect uptake efficiency and RalA is not activated in response to large particles. Fig. S5 shows the localization pattern of exocyst complex components. Table S1 shows expression plasmids used in this study. Video 1 shows cell spreading on invasin-coated glass surface in control and Cdc42-depleted cells. Video 2 shows ratiometric imaging to quantify Cdc42 activity at small nascent phagosomes. Video 3 shows ratiometric imaging to quantify Cdc42 activity at large nascent phagosomes. Video 4 shows small phagosome morphology in cells expressing Cdc42. Video 5 shows small phagosome morphology in Cdc42-depleted cells. Video 6 shows large phagosome morphology in cells expressing Cdc42. Video 7 shows large phagosome morphology in Cdc42-depleted cells. Online supplemental material is available at http://www.jcb.org/cgi/content/full/jcb.201204090/DC1.

We would like to thank Larry Feig, Ka-Wing Wong, and Elizabeth Creasey for helpful discussions and members of the Isberg laboratory for critical review

of the text. We thank Emmanuelle Caron, Scott Snapper, Joel Swanson, Tobias Meyer, and Larry Feig for providing reagents.

This work was supported by Howard Hughes Medical Institute, by award R37AI23538 and training grant 5T32AI007422 from the National Institute of Allergy and Infectious Diseases, and by Program Project Award grant P30DK34928 from the National Institute of Diabetes and Digestive and Kidney Diseases.

Submitted: 17 April 2012
Accepted: 5 December 2012

References

Aderem, A., and D.M. Underhill. 1999. Mechanisms of phagocytosis in macrophages. *Annu. Rev. Immunol.* 17:593–623. http://dx.doi.org/10.1146/annurev.immunol.17.1.593

Alrutz, M.A., A. Srivastava, K.W. Wong, C. D'Souza-Schorey, M. Tang, L.E. Ch'Ng, S.B. Snapper, and R.R. Isberg. 2001. Efficient uptake of *Yersinia pseudotuberculosis* via integrin receptors involves a Rac1-Arp 2/3 pathway that bypasses N-WASP function. *Mol. Microbiol.* 42:689–703. http://dx.doi.org/10.1046/j.1365-2958.2001.02676.x

Bajno, L., X.R. Peng, A.D. Schreiber, H.P. Moore, W.S. Trimble, and S. Grinstein. 2000. Focal exocytosis of VAMP3-containing vesicles at sites of phagosome formation. *J. Cell Biol.* 149:697–706. http://dx.doi.org/10.1083/jcb.149.3.697

Beemiller, P., Y. Zhang, S. Mohan, E. Levinsohn, I. Gaeta, A.D. Hoppe, and J.A. Swanson. 2010. A Cdc42 activation cycle coordinated by PI 3-kinase during Fc receptor-mediated phagocytosis. *Mol. Biol. Cell*. 21:470–480. http://dx.doi.org/10.1091/mbc.E08-05-0494

Caron, E., and A. Hall. 1998. Identification of two distinct mechanisms of phagocytosis controlled by different Rho GTPases. *Science*. 282:1717–1721. http://dx.doi.org/10.1126/science.282.5394.1717

Chan, A.Y., S.J. Coniglio, Y.Y. Chuang, D. Michaelson, U.G. Knaus, M.R. Philips, and M. Symons. 2005. Roles of the Rac1 and Rac3 GTPases in human tumor cell invasion. *Oncogene*. 24:7821–7829. http://dx.doi.org/10.1038/sj.onc.1208909

Clark, E.A., W.G. King, J.S. Brugge, M. Symons, and R.O. Hynes. 1998. Integrin-mediated signals regulated by members of the rho family of GTPases. *J. Cell Biol.* 142:573–586. http://dx.doi.org/10.1083/jcb.142.2.573

Cougoule, C., A. Wiedemann, J. Lim, and E. Caron. 2004. Phagocytosis, an alternative model system for the study of cell adhesion. *Semin. Cell Dev. Biol.* 15:679–689.

Cox, D., C.C. Tseng, G. Bjekic, and S. Greenberg. 1999. A requirement for phosphatidylinositol 3-kinase in pseudopod extension. *J. Biol. Chem.* 274:1240–1247. http://dx.doi.org/10.1074/jbc.274.3.1240

Cox, D., D.J. Lee, B.M. Dale, J. Calafat, and S. Greenberg. 2000. A Rab11-containing rapidly recycling compartment in macrophages that promotes phagocytosis. *Proc. Natl. Acad. Sci. USA*. 97:680–685. http://dx.doi.org/10.1073/pnas.97.2.680

Das, A., and W. Guo. 2011. Rabs and the exocyst in ciliogenesis, tubulogenesis and beyond. *Trends Cell Biol.* 21:383–386. http://dx.doi.org/10.1016/j.tcb.2011.03.006

Dupuy, A.G., and E. Caron. 2008. Integrin-dependent phagocytosis: spreading from microadhesion to new concepts. *J. Cell Sci.* 121:1773–1783. http://dx.doi.org/10.1242/jcs.018036

Eden, S., R. Rohatgi, A.V. Podtelejnikov, M. Mann, and M.W. Kirschner. 2002. Mechanism of regulation of WAVE1-induced actin nucleation by Rac1 and Nck. *Nature*. 418:790–793. http://dx.doi.org/10.1038/nature00859

Garrett, W.S., L.M. Chen, R. Kroschewski, M. Ebersold, S. Turley, S. Trombetta, J.E. Galán, and I. Mellman. 2000. Developmental control of endocytosis in dendritic cells by Cdc42. *Cell*. 102:325–334. http://dx.doi.org/10.1016/S0092-8674(00)00038-6

Gauthier, N.C., O.M. Rossier, A. Mathur, J.C. Hone, and M.P. Sheetz. 2009. Plasma membrane area increases with spread area by exocytosis of a GPI-anchored protein compartment. *Mol. Biol. Cell*. 20:3261–3272. http://dx.doi.org/10.1091/mbc.E09-01-0071

Henry, R.M., A.D. Hoppe, N. Joshi, and J.A. Swanson. 2004. The uniformity of phagosome maturation in macrophages. *J. Cell Biol.* 164:185–194. http://dx.doi.org/10.1083/jcb.200307080

Holevinsky, K.O., and D.J. Nelson. 1998. Membrane capacitance changes associated with particle uptake during phagocytosis in macrophages. *Biophys. J.* 75:2577–2586. http://dx.doi.org/10.1016/S0006-3495(98)77703-3

Huynh, K.K., J.G. Kay, J.L. Stow, and S. Grinstein. 2007. Fusion, fission, and secretion during phagocytosis. *Physiology (Bethesda)*. 22:366–372. http://dx.doi.org/10.1152/physiol.00028.2007

Hynes, R.O. 2002. Integrins: bidirectional, allosteric signaling machines. *Cell*. 110:673–687. http://dx.doi.org/10.1016/S0092-8674(02)00971-6

Inoue, M., L. Chang, J. Hwang, S.H. Chiang, and A.R. Saltiel. 2003. The exocyst complex is required for targeting of Glut4 to the plasma membrane by insulin. *Nature*. 422:629–633. http://dx.doi.org/10.1038/nature01533

Kerr, J.F., A.H. Wyllie, and A.R. Currie. 1972. Apoptosis: a basic biological phenomenon with wide-ranging implications in tissue kinetics. *Br. J. Cancer*. 26:239–257. http://dx.doi.org/10.1038/bjc.1972.33

Kim, S., K. Shilagardi, S. Zhang, S.N. Hong, K.L. Sens, J. Bo, G.A. Gonzalez, and E.H. Chen. 2007. A critical function for the actin cytoskeleton in targeted exocytosis of prefusion vesicles during myoblast fusion. *Dev. Cell*. 12:571–586. http://dx.doi.org/10.1016/j.devcel.2007.02.019

Kroschewski, R., A. Hall, and I. Mellman. 1999. Cdc42 controls secretory and endocytic transport to the basolateral plasma membrane of MDCK cells. *Nat. Cell Biol.* 1:8–13. http://dx.doi.org/10.1038/8977

Krysko, D.V., G. Denecker, N. Festjens, S. Gabriels, E. Parthoens, K. D'Herde, and P. Vandenabeele. 2006. Macrophages use different internalization mechanisms to clear apoptotic and necrotic cells. *Cell Death Differ.* 13:2011–2022. http://dx.doi.org/10.1038/sj.cdd.4401900

Leverrier, Y., and A.J. Ridley. 2001. Requirement for Rho GTPases and PI 3-kinases during apoptotic cell phagocytosis by macrophages. *Curr. Biol.* 11:195–199. http://dx.doi.org/10.1016/S0960-9822(01)00047-1

Leverrier, Y., R. Lorenzi, M.P. Blundell, P. Brickell, C. Kinnon, A.J. Ridley, and A.J. Thrasher. 2001. Cutting edge: the Wiskott-Aldrich syndrome protein is required for efficient phagocytosis of apoptotic cells. *J. Immunol.* 166:4831–4834.

Lin, R., S. Bagrodia, R. Cerione, and D. Manor. 1997. A novel Cdc42Hs mutant induces cellular transformation. *Curr. Biol.* 7:794–797. http://dx.doi.org/10.1016/S0960-9822(06)00338-1

Lipschutz, J.H., and K.E. Mostov. 2002. Exocytosis: the many masters of the exocyst. *Curr. Biol.* 12:R212–R214. http://dx.doi.org/10.1016/S0960-9822(02)00753-4

Liu, J., X. Zuo, P. Yue, and W. Guo. 2007. Phosphatidylinositol 4,5-bisphosphate mediates the targeting of the exocyst to the plasma membrane for exocytosis in mammalian cells. *Mol. Biol. Cell*. 18:4483–4492. http://dx.doi.org/10.1091/mbc.E07-05-0461

Liu, J., Y. Zhao, Y. Sun, B. He, C. Yang, T. Svitkina, Y.E. Goldman, and W. Guo. 2012. Exo70 stimulates the Arp2/3 complex for lamellipodia formation and directional cell migration. *Curr. Biol.* 22:1510–1515. http://dx.doi.org/10.1016/j.cub.2012.05.055

Matern, H.T., C. Yeaman, W.J. Nelson, and R.H. Scheller. 2001. The Sec6/8 complex in mammalian cells: characterization of mammalian Sec3, subunit interactions, and expression of subunits in polarized cells. *Proc. Natl. Acad. Sci. USA*. 98:9648–9653. http://dx.doi.org/10.1073/pnas.171317898

Mohammadi, S., and R.R. Isberg. 2009. *Yersinia pseudotuberculosis* virulence determinants invasin, YopE, and YopT modulate RhoG activity and localization. *Infect. Immun.* 77:4771–4782. http://dx.doi.org/10.1128/IAI.00850-09

Munson, M., and P. Novick. 2006. The exocyst defrocked, a framework of rods revealed. *Nat. Struct. Mol. Biol.* 13:577–581. http://dx.doi.org/10.1038/nsmb1097

Nagata, S. 2007. Autoimmune diseases caused by defects in clearing dead cells and nuclei expelled from erythroid precursors. *Immunol. Rev.* 220:237–250. http://dx.doi.org/10.1111/j.1600-065X.2007.00571.x

Nichols, C.D., and J.E. Casanova. 2010. *Salmonella*-directed recruitment of new membrane to invasion foci via the host exocyst complex. *Curr. Biol.* 20:1316–1320. http://dx.doi.org/10.1016/j.cub.2010.05.065

Niedergang, F., and P. Chavrier. 2005. Regulation of phagocytosis by Rho GTPases. *Curr. Top. Microbiol. Immunol.* 291:43–60. http://dx.doi.org/10.1007/3-540-27511-8_4

Nobes, C.D., and A. Hall. 1995. Rho, rac, and cdc42 GTPases regulate the assembly of multimolecular focal complexes associated with actin stress fibers, lamellipodia, and filopodia. *Cell*. 81:53–62. http://dx.doi.org/10.1016/0092-8674(95)90370-4

Park, H., and D. Cox. 2009. Cdc42 regulates Fc gamma receptor-mediated phagocytosis through the activation and phosphorylation of Wiskott-Aldrich syndrome protein (WASP) and neural-WASP. *Mol. Biol. Cell*. 20:4500–4508. http://dx.doi.org/10.1091/mbc.E09-03-0230

Partridge, M.A., and E.E. Marcantonio. 2006. Initiation of attachment and generation of mature focal adhesions by integrin-containing filopodia in cell spreading. *Mol. Biol. Cell*. 17:4237–4248. http://dx.doi.org/10.1091/mbc.E06-06-0496

Patel, J.C., and J.E. Galán. 2006. Differential activation and function of Rho GTPases during *Salmonella*–host cell interactions. *J. Cell Biol.* 175:453–463. http://dx.doi.org/10.1083/jcb.200605144

Price, L.S., J. Leng, M.A. Schwartz, and G.M. Bokoch. 1998. Activation of Rac and Cdc42 by integrins mediates cell spreading. *Mol. Biol. Cell*. 9:1863–1871.

Prigent, M., T. Dubois, G. Raposo, V. Derrien, D. Tenza, C. Rossé, J. Camonis, and P. Chavrier. 2003. ARF6 controls post-endocytic recycling through its downstream exocyst complex effector. *J. Cell Biol.* 163:1111–1121. http://dx.doi.org/10.1083/jcb.200305029

Rankin, S., R.R. Isberg, and J.M. Leong. 1992. The integrin-binding domain of invasin is sufficient to allow bacterial entry into mammalian cells. *Infect. Immun.* 60:3909–3912.

Ren, M., G. Xu, J. Zeng, C. De Lemos-Chiarandini, M. Adesnik, and D.D. Sabatini. 1998. Hydrolysis of GTP on rab11 is required for the direct delivery of transferrin from the pericentriolar recycling compartment to the cell surface but not from sorting endosomes. *Proc. Natl. Acad. Sci. USA*. 95:6187–6192. http://dx.doi.org/10.1073/pnas.95.11.6187

Ren, Y., and J. Savill. 1998. Apoptosis: the importance of being eaten. *Cell Death Differ.* 5:563–568. http://dx.doi.org/10.1038/sj.cdd.4400407

Rohatgi, R., P. Nollau, H.Y. Ho, M.W. Kirschner, and B.J. Mayer. 2001. Nck and phosphatidylinositol 4,5-bisphosphate synergistically activate actin polymerization through the N-WASP-Arp2/3 pathway. *J. Biol. Chem.* 276:26448–26452. http://dx.doi.org/10.1074/jbc.M103856200

Sakurai-Yageta, M., C. Recchi, G. Le Dez, J.B. Sibarita, L. Daviet, J. Camonis, C. D'Souza-Schorey, and P. Chavrier. 2008. The interaction of IQGAP1 with the exocyst complex is required for tumor cell invasion downstream of Cdc42 and RhoA. *J. Cell Biol.* 181:985–998. http://dx.doi.org/10.1083/jcb.200709076

Savill, J., I. Dransfield, C. Gregory, and C. Haslett. 2002. A blast from the past: clearance of apoptotic cells regulates immune responses. *Nat. Rev. Immunol.* 2:965–975. http://dx.doi.org/10.1038/nri957

Savina, A., and S. Amigorena. 2007. Phagocytosis and antigen presentation in dendritic cells. *Immunol. Rev.* 219:143–156. http://dx.doi.org/10.1111/j.1600-065X.2007.00552.x

Shaner, N.C., R.E. Campbell, P.A. Steinbach, B.N. Giepmans, A.E. Palmer, and R.Y. Tsien. 2004. Improved monomeric red, orange and yellow fluorescent proteins derived from *Discosoma* sp. red fluorescent protein. *Nat. Biotechnol.* 22:1567–1572. http://dx.doi.org/10.1038/nbt1037

Stuart, L.M., J. Boulais, G.M. Charriere, E.J. Hennessy, S. Brunet, I. Jutras, G. Goyette, C. Rondeau, S. Letarte, H. Huang, et al. 2007. A systems biology analysis of the *Drosophila* phagosome. *Nature*. 445:95–101. http://dx.doi.org/10.1038/nature05380

Sugihara, K., S. Asano, K. Tanaka, A. Iwamatsu, K. Okawa, and Y. Ohta. 2002. The exocyst complex binds the small GTPase RalA to mediate filopodia formation. *Nat. Cell Biol.* 4:73–78. http://dx.doi.org/10.1038/ncb720

Swanson, J.A. 2008. Shaping cups into phagosomes and macropinosomes. *Nat. Rev. Mol. Cell Biol.* 9:639–649. http://dx.doi.org/10.1038/nrm2447

Symons, M., J.M. Derry, B. Karlak, S. Jiang, V. Lemahieu, F. Mccormick, U. Francke, and A. Abo. 1996. Wiskott-Aldrich syndrome protein, a novel effector for the GTPase CDC42Hs, is implicated in actin polymerization. *Cell*. 84:723–734. http://dx.doi.org/10.1016/S0092-8674(00)81050-8

Takahashi, S., K. Kubo, S. Waguri, A. Yabashi, H.W. Shin, Y. Katoh, and K. Nakayama. 2012. Rab11 regulates exocytosis of recycling vesicles at the plasma membrane. *J. Cell Sci.* 125:4049–4057. http://dx.doi.org/10.1242/jcs.102913

TerBush, D.R., T. Maurice, D. Roth, and P. Novick. 1996. The Exocyst is a multiprotein complex required for exocytosis in *Saccharomyces cerevisiae*. *EMBO J.* 15:6483–6494.

Teruel, M.N., T.A. Blanpied, K. Shen, G.J. Augustine, and T. Meyer. 1999. A versatile microporation technique for the transfection of cultured CNS neurons. *J. Neurosci. Methods*. 93:37–48. http://dx.doi.org/10.1016/S0165-0270(99)00112-0

Tran Van Nhieu, G., and R.R. Isberg. 1993. Bacterial internalization mediated by beta 1 chain integrins is determined by ligand affinity and receptor density. *EMBO J.* 12:1887–1895.

van Dam, E.M., and P.J. Robinson. 2006. Ral: mediator of membrane trafficking. *Int. J. Biochem. Cell Biol.* 38:1841–1847. http://dx.doi.org/10.1016/j.biocel.2006.04.006

van Ijzendoorn, S.C. 2006. Recycling endosomes. *J. Cell Sci.* 119:1679–1681. http://dx.doi.org/10.1242/jcs.02948

Vaux, D.L., and S.J. Korsmeyer. 1999. Cell death in development. *Cell*. 96:245–254. http://dx.doi.org/10.1016/S0092-8674(00)80564-4

Wang, T., Z. Ming, W. Xiaochun, and W. Hong. 2011. Rab7: role of its protein interaction cascades in endo-lysosomal traffic. *Cell. Signal.* 23:516–521. http://dx.doi.org/10.1016/j.cellsig.2010.09.012

Wiedemann, A., S. Linder, G. Grassl, M. Albert, I. Autenrieth, and M. Aepfelbacher. 2001. *Yersinia enterocolitica* invasin triggers phagocytosis via beta1 integrins, CDC42Hs and WASp in macrophages. *Cell. Microbiol.* 3:693–702. http://dx.doi.org/10.1046/j.1462-5822.2001.00149.x

Wilkinson, S., H.F. Paterson, and C.J. Marshall. 2005. Cdc42-MRCK and Rho-ROCK signalling cooperate in myosin phosphorylation and cell invasion. *Nat. Cell Biol.* 7:255–261. http://dx.doi.org/10.1038/ncb1230

Wong, K.W., and R.R. Isberg. 2005. *Yersinia pseudotuberculosis* spatially controls activation and misregulation of host cell Rac1. *PLoS Pathog.* 1:e16. http://dx.doi.org/10.1371/journal.ppat.0010016

Wu, H., C. Turner, J. Gardner, B. Temple, and P. Brennwald. 2010. The Exo70 subunit of the exocyst is an effector for both Cdc42 and Rho3 function in polarized exocytosis. *Mol. Biol. Cell*. 21:430–442. http://dx.doi.org/10.1091/mbc.E09-06-0501

Zeng, J., M. Ren, D. Gravotta, C. De Lemos-Chiarandini, M. Lui, H. Erdjument-Bromage, P. Tempst, G. Xu, T.H. Shen, T. Morimoto, et al. 1999. Identification of a putative effector protein for rab11 that participates in transferrin recycling. *Proc. Natl. Acad. Sci. USA*. 96:2840–2845. http://dx.doi.org/10.1073/pnas.96.6.2840

Zhang, X., E. Bi, P. Novick, L. Du, K.G. Kozminski, J.H. Lipschutz, and W. Guo. 2001. Cdc42 interacts with the exocyst and regulates polarized secretion. *J. Biol. Chem.* 276:46745–46750. http://dx.doi.org/10.1074/jbc.M107464200

Zhang, X.M., S. Ellis, A. Sriratana, C.A. Mitchell, and T. Rowe. 2004. Sec15 is an effector for the Rab11 GTPase in mammalian cells. *J. Biol. Chem.* 279:43027–43034. http://dx.doi.org/10.1074/jbc.M402264200

Zuo, X., J. Zhang, Y. Zhang, S.C. Hsu, D. Zhou, and W. Guo. 2006. Exo70 interacts with the Arp2/3 complex and regulates cell migration. *Nat. Cell Biol.* 8:1383–1388. http://dx.doi.org/10.1038/ncb1505

Zuo, X., B. Fogelgren, and J.H. Lipschutz. 2011. The small GTPase Cdc42 is necessary for primary ciliogenesis in renal tubular epithelial cells. *J. Biol. Chem.* 286:22469–22477. http://dx.doi.org/10.1074/jbc.M111.238469